ELSEVIER

Contents lists available at ScienceDirect

Materials & Design

journal homepage: www.elsevier.com/locate/matdes





Additive manufacturing with continuous ultra-high molecular weight polyethylene yarn

Colin Marquis^a, Renjie Song^a, Sarah Waddell^a, Andy Luong^a, Dwayne Arola^{a,b,*}

- a Materials Science Engineering, University of Washington, Seattle, USA
- ^b Mechanical Engineering, University of Washington, Seattle, USA

ARTICLE INFO

Keywords: Additive manufacturing Composite Fused filament fabrication UHMWPE

ABSTRACT

Fused filament fabrication (FFF) of composites with compliant high-strength fibers could expand opportunities for the design and fabrication of complex flexible structures, but this topic has received limited attention. This study pursued the development of filaments consisting of ultra-high molecular weight polyethylene yarn (UHMWPE) embedded in a matrix of polycaprolactone (UPE/PCL) and successful 3D printing. The physical characteristics and printability of the filament were evaluated in terms of key parameters including spooling speed, temperature, fiber distribution (consolidated vs dispersed), and fiber volume fraction (4 \leq V $_{\rm f}$ \leq 30 %). An evaluation of the microstructure and tensile properties of the UPE/PCL was performed after processing and printing. Prior to printing, the filament exhibited an ultimate tensile strength (UTS) of 590 \pm 40 MPa with apparent fiber strength of 2.4 GPa. For the printed condition, the UTS reached 470 \pm 60 MPa and apparent fiber strength of 1.9 GPa. Fiber dispersion in the filament plays an important role on the printed properties and the potential for fiber degradation. Nevertheless, the strength of the UPE/PCL represents a new performance benchmark for compliant composites printed by FFF. This new material system can support applications where strength and toughness are key performance metrics in addition to flexibility.

1. Introduction

Additive manufacturing (AM) processes have undergone nearly unrivaled growth in recent years [1,2]. The ability to fabricate parts through layer-by-layer deposition of material enables physical net-shape parts to be produced directly from a computer aided design (CAD) model. AM processes have provided engineers with an approach to manufacturing that has few design constraints and overcomes many challenges associated with traditional methods [3]. Clearly, AM has the potential to radically disrupt existing approaches to the production of consumer goods and the world's manufacturing supply chains [4]. A key to capitalizing on these opportunities is the development of new materials that expand the range of products, their performance, and the possibilities for application [5].

Fused filament fabrication (FFF), often referred to as threedimensional (3D) printing, is one of the most ubiquitous of the AM processes available today. While commonly sought for printing thermoplastics, there is rapid growth in FFF of composite materials involving fibers and a thermoplastic matrix [6,7]. Printing with composite materials could enable the manufacture of components with high specific strength and significantly less waste than customary for a traditional wet layup with thermoset matrix systems [8].

Currently, the filaments available for FFF of composites are relatively limited; the majority possess reinforcements with both high stiffness and strength [7,9,10]. For instance, commercial feedstocks are available for FFF with chopped fibers of carbon [11], glass [12], and Kevlar [13]. Fewer filaments are available for performing FFF with continuous fibers [7]. Based on the principles of mechanics, continuous fiber reinforcements are more effective in distributing stress among the fibers and can achieve higher strength [14,15,16,17]. As such, there is substantial interest in the development of filaments with continuous fibers [18]

Challenges to producing and printing filaments with continuous fibers has tempered the rate of advancements in AM of composites by FFF [10,19]. Parker et al. recently reported on FFF with experimental filaments of continuous carbon fiber (CCF) and polyphenylene sulfide (PPS) matrix, with up to 50 % volume fraction (V_f) reinforcement [20]. The printed strengths reached 2 GPa, which highlights the incredible possibilities in FFF of composites. Nevertheless, that strength is difficult to achieve with high reliability. Previous studies have explored the

^{*} Corresponding author at: Department of Materials and Engineering, University of Washington, Roberts Hall, 333, Seattle, WA 98195-2120. E-mail address: darola@uw.edu (D. Arola).

printing of filaments with CCFs and different thermoplastic matrices, while others have focused on optimizing tool paths for 3D printing composites with CCFs, all of which are largely directed to maximize the strength of the printed material [21,22,23]. Composite filaments with high stiffness continuous fibers are generally brittle and susceptible to damage during FFF, which can reduce the printed strength relative to that prior to printing [20,24]. Composites with compliant fibers should be less susceptible to damage in FFF, yet reported studies involving material systems with compliant fibers are scanty.

To the authors knowledge, no study has reported on the development of filaments for FFF with high strength compliant fibers and validated their printability. Interesting studies have reported printing of composite filaments with natural fibers such as flax and jute, but the strengths are limited. Printing with flax fibers reported by Zhang et al. achieved a maximum UTS of approximately 90 MPa, whereas printing with jute fibers reported by Matsuzaki et al. achieved an UTS approaching 60 MPa [25,26,27]. The jute fibers were embedded into the thermoplastic within the nozzle assembly, while the flax fibers were introduced in a separate filament fabrication step. One limitation of past studies is the low $V_{\rm f}$; the jute fiber filament contained 6.1 % fibers, a small fraction of that common of composite filaments in aerospace with $V_{\rm f} \geq 50$ %.

The design possibilities for high strength compliant fiber filaments are abundant. Most components that require flexibility currently lack the strength required for applications beyond prototyping. Stiff fiber reinforcements pose a penalty to design as tool paths must accommodate the brittle fibers [24]. Huang et al. [28] presented special tool paths for stiff fiber reinforcements. In contrast, no special modifications should be required for the tool paths in printing compliant fiber systems. Composites with continuous compliant fibers could greatly advance the development of 3D-printed complaint mechanisms and expand the design envelope. An excellent example was presented by Liu et al. [29] for robotic grips where both strength and flexibility are required.

The overall objective of this investigation was to develop filaments of continuous fiber reinforced thermoplastic for FFF with high strength compliant fibers and assess the printability as well as the mechanical properties pre- and post-printing. The specific aims were to: i) evaluate the role of different manufacturing parameters during filament fabrication, ii) examine the microstructure and mechanical properties of this new material and factors contributing to its performance, and iii) evaluate the printability of the filaments in the fabrication of single and multilayer structures. Filaments were produced with tows of Ultra High Molecular Weight Polyethylene (UHMWPE) multi-fiber varn and a compatible matrix and then printed using FFF. This study is the first to produce and characterize a continuous UHMWPE fiber composite filament for FFF. As such, the contributions of this report of findings fill a current gap in the AM materials space and the new feedstock has potential applications in medical grade prosthetics, wearable electronics, and next generation flexible armors. The results provide insight into manufacturing challenges associated with a material system of this class and the potential for this filament to address gaps in AM feedstocks where high specific strength, toughness, and flexibility are key.

2. Materials and methods

The filaments produced in this investigation consisted of a tow of commercially available UHMWPE yarn (SK99 dtex 880 Dyneema, DSM, Greenville, North Carolina), and a 50,000 AMU grade polycaprolactone (PCL) matrix (Material Sample Shop, Futation, Denmark). The composite of UHMWPE and PCL is referred to here as UPE/PCL.

UHMWPE is recognized for its high strength to weight ratio, as well as its resistance to abrasion, impact, and chemical degradation [30]. The fibers are up to 15 times stronger than steel for equivalent mass, making it an attractive reinforcement for composites where strength to weight ratio is critical [30]. However, UHMWPE fibers pose a substantial challenge to the FFF process due to their low stiffness, low melting point

(144–152 °C), and susceptibility to damage at temperatures of 80–100 °C [31]. As such, a thermoplastic matrix with low melting point is required to avoid fiber degradation. Amza et al. laid UHMWPE fibers by hand between print layers of polylactic acid (PLA), but the high melting temperature of PLA (170–180 °C) prevented the successful development of a filament with those constituents [32]. In the present effort a biodegradable polyester matrix of PCL was chosen to assess the printability. With a melting point of 60 °C, introduction of the fibers is possible without extensive thermal damage to the fiber tow.

2.1. Filament fabrication

Filaments were fabricated using a pultrusion technique (Fig. 1). The fiber tow was passed under a series of guiding rods through a heated bath of PCL at 75 °C. The fibers were encapsulated within the PCL while being pulled through the length of the bath, akin to Matsuzaki et al. [33]. The UPE yarn was pulled through a printing nozzle mounted at the forward end of the tank. Brass nozzles ranging in internal diameter from 0.6 mm to 2 mm were explored. The extruded composite filament was cooled by forced convection using fans placed below the exiting filament to remove residual heat. The filament was spooled using a Filabot Spooler (Precision Filament Winder, FB00073, Vermont) and the filament was wound around an empty spool. Due to the high viscosity of PCL at 75 °C, it was necessary to maintain control of the PCL in the resin tank to ensure uniform impregnation of the fibers. As the fibers exit the tank nozzle the internal diameter of the nozzle removes excess PCL. The slow spooling speeds used to produce the composite filaments resulted in fiber exposure temperatures that were highest just before exiting the tank nozzle. As such, temperature measurements were performed using a thermocouple mounted at the tank nozzle assembly.

A preliminary analysis of the effects of temperature and spooling speed on the resulting fiber V_f and fiber distribution was conducted to enable consistent filament production. Spooling speeds ranging from 0.2 to 0.75 cm/sec were employed as well as bath temperatures of 75 to 140 $^{\circ}$ C. The fiber V_f of the filament was estimated using the cross-sectional area of the dtex 880 fiber tow divided by the cross-sectional area of the filament.

Based on preliminary experiments, the spooling speed was identified as an important factor to the filament qualities. Filaments spooled more quickly resulted in higher fiber volume fractions due to a decrease in PCL matrix coating the fiber tow. This is likely caused by viscous effects at the tank nozzle exit. However, faster spooling speeds resulted in less dispersion of the fibers within the matrix, often resulting in a densely packed fiber bundle at the center of the filament. Dispersion of the fibers within the PCL matrix tank is critical to homogenizing their distribution within the filament. Sequential processing and analysis showed that the redistribution is more consistent at slower spooling speeds, as expected, where there was ample time to redistribute the fibers. However, tank temperatures above 140 °C resulted in visible damage to the Dyneema fiber tow when using slow spooling speeds. Specifically, individual fibers would cleave at the PCL-air interface. Damage to the fiber tow has been shown to be detrimental to the mechanical performance of continuous fiber composites [24]. Guided by results of these preliminary experiments, the filaments prepared for mechanical testing were produced using a 75 $^{\circ}$ C PCL bath temperature, a 0.8 mm tank nozzle, and a spooling speed of ~ 0.25 cm/s.

The microstructure of the filaments was evaluated before and after printing using an optical microscope (Model BX51M, Olympus Corporation, Tokyo, Japan) with an attached digital camera (1024×768 resolution). Samples were mounted in Epofix HQ Resin and Hardener and polished in a successive series beginning at #400 grit and ending at #1200 grit polishing pads. Cross sections were examined using 5x magnification and evaluated using ImageJ (V1.53 t 24, National Institutes of Health, USA). When appropriate, Gaussian fits were performed to quantitatively describe the distribution of individual fibers within the filaments with and without fiber dispersion. The fits were

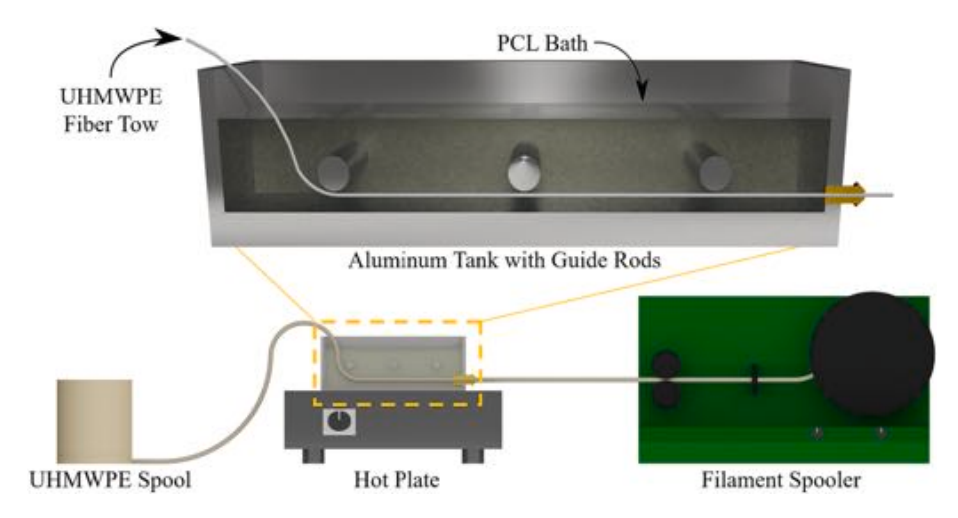


Fig. 1. Filament fabrication process showing UHMWPE fiber tow in the PCL bath.

obtained according to:

$$G(x) = Ae^{\frac{-(x-\mu)^2}{2\sigma^2}}$$
 (1)

where G(x) is the least squares fit gaussian profile, x defines the distance from the centroid, A represents the profile amplitude, μ signifies the midpoint, and σ is the standard deviation.

2.2. Printing

Printing of the filaments was conducted using a Prusa Model I3 MK3S for fused filament fabrication (Prague, Czech Republic). The Prusa heater block was rewired from the printer to an independent temperature controller (OMRON, E5CB, Kyoto, Japan) and powered by a 24 V DC, 15 Amp switch power supply. A Type K thermocouple was attached to the heater block and connected to the temperature controller. Printing was performed using a 1.2 mm brass nozzle at 120 °C at a rate of 100 mm/min (Fig. 2) on a 0.5 mm thick spring steel print bed (FYSETC, Guangdong, China). According to results of preliminary printing experiments, a temperature of 120 °C was selected to enable high quality printing of the PCL matrix with minimal thermal damage to the UPE yarn. A speed of 100 mm/min was chosen to minimize the time of the UPE/PCL in the nozzle assembly while providing a speed achievable by most consumer grade 3D printers.



Fig. 2. Printing of 0.8 mm filament with dispersed fibers using a 1.2 mm brass nozzle.

2.3. Mechanical testing

Mechanical testing was conducted under uniaxial tension on the neat UHMWPE yarn and the UPE/PCL filaments before and after printing using an Instron E1000 load frame (Instron Corporation, E1000, Morwood, MA, USA). Testing of individual filaments was selected instead of sample coupons to better characterize the materials science contributions to the mechanical properties rather than the behavior of a larger connective structure. Special fixtures were developed for the purpose of axial loading following designs used for tensile testing of braided ropes as shown in Fig. 3 [34].

The grips were fabricated using Markforged Onyx material with $55\,\%$ infill. The Dyneema fibers and UPE/PCL filaments were wrapped once around the fixture posts to prevent slipping during uniaxial loading. The samples prepared for testing were roughly 700 mm in length and were clamped between the surface of the grips and a metal backing plate with sandpaper used to aid in friction. A total of 15 samples were prepared for each material and processing condition.

Tensile testing was conducted in displacement control at a ramp rate of 5 mm/min with a gauge length of ~ 145 mm. The performance of the filament was examined before and after printing in terms of the ultimate tensile strength (UTS) and the modulus of toughness (MOT). The MOT was computed using a trapezoidal sum to compute the area under the stress-strain curve up to the strain corresponding to the UTS. The strain response was estimated from the machine elongation, accounting for the grip and machine compliance.

The stress used in computing the UTS and MOT was calculated in two different ways. The first approach defines the composite strength, which was simply the load divided by the cross-section area of the filament. The second approach concentrates on the stress in the fibers, termed the apparent fiber strength. The PCL matrix has an average elastic modulus and UTS of 364 MPa and 16 MPa, respectively, whereas the Dyneema has a reported elastic modulus and UTS of 155 GPa and approximately 4 GPa, respectively [35,36]. Due to the low elastic modulus and strength of the PCL, the fibers carry the majority of load in the UPE/PCL filaments. Hence, to assess damage to the load-carrying capacity of the fibers, the "apparent fiber strength" (i.e. the UTS of the fibers at failure) was estimated using the $V_{\rm f}$ of the filaments and rule of mixtures according to

$$UTS_{fiber} = \frac{UTS_{Composite} - (1 - V_f) \bullet UTS_{matrix}}{V_f}$$
 (2)

where all strength terms are defined in terms of their associated subscript and the V_f is the volume fraction of UHMWPE fibers.

Another important quality of the filament was the statistical distri-

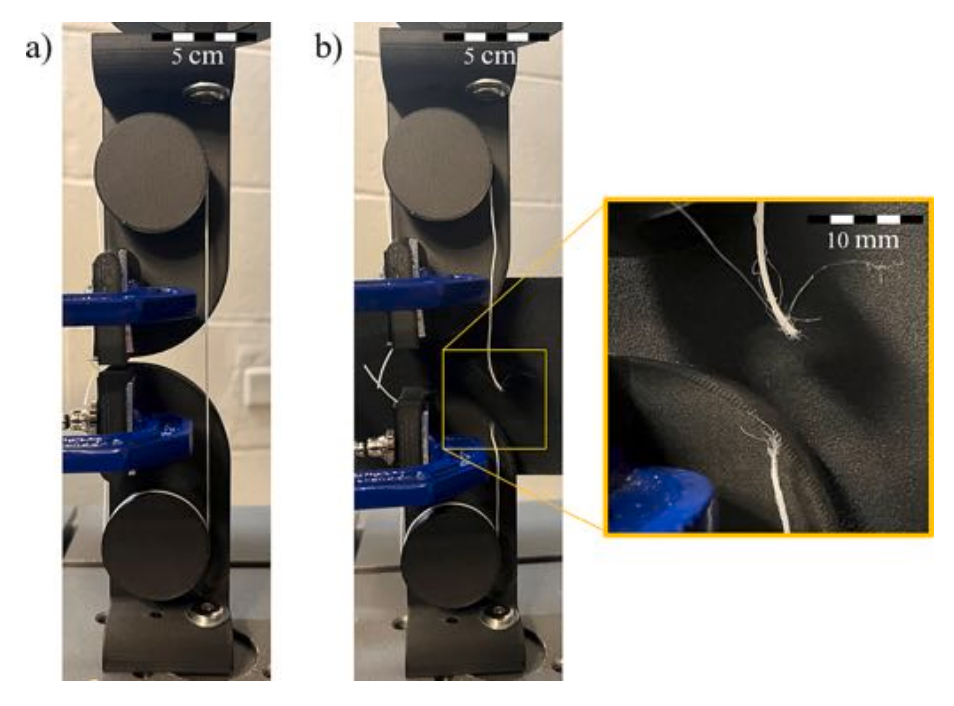


Fig. 3. Tensile testing of UPE/PCL using the dedicated fixtures. a) UPE/PCL filament undergoing uniaxial tensile testing while under load. b) Filament after failure in gauge section.

bution in strength. Fiber damage caused by filament fabrication and/or printing can reduce the strength and cause an increase in variability due the number and size of defects. Hence, a two-parameter Weibull analysis was performed with the strengths according to

$$P(\sigma) = 1 - exp\left(-\left(\frac{\sigma}{\sigma_{\circ}}\right)\right)^{m} \tag{3}$$

where $P(\sigma)$ represents the probability of failure at the axial stress $(\sigma),$ m is the Weibull modulus, and σ_0 is the characteristic strength. The probability of failure (P_f) was defined according to the estimator function described as

$$P_f(i) = \frac{(i - 0.5)}{N} \tag{4}$$

where i and N represent the ith sample in the ranking and the total sample count in the group, respectively. The Weibull parameters were obtained for the filaments evaluated before and after printing and for the

filaments produced with dispersed and non-dispersed fiber distributions. A comparison of the Weibull parameters was performed to understand the contributions of processing to variability in strength.

3. Results

Fig. 4 presents the fiber V_f distribution of the UPE/PCL filaments over the parameter space used in their development. The filaments produced using the 0.8 mm and 2 mm diameter nozzles had mean fiber volume fractions of 24 % and 7 %, respectively. Ignoring shrinkage of the PCL after exiting the tank nozzle and other viscous effects, the limiting V_f (theoretical minimum) for these two nozzle diameters is 18 % and 3 %, respectively. The experimentally measured V_f is larger than the theoretical minimum estimated from the nozzle diameter, which demonstrates that viscous effects and shrinkage play an important role on the final cross-sectional area of the filaments. Interestingly, the raw variability in V_f for the filaments produced using the 0.8 mm nozzle was smaller than that compared to the 2 mm nozzle. The population

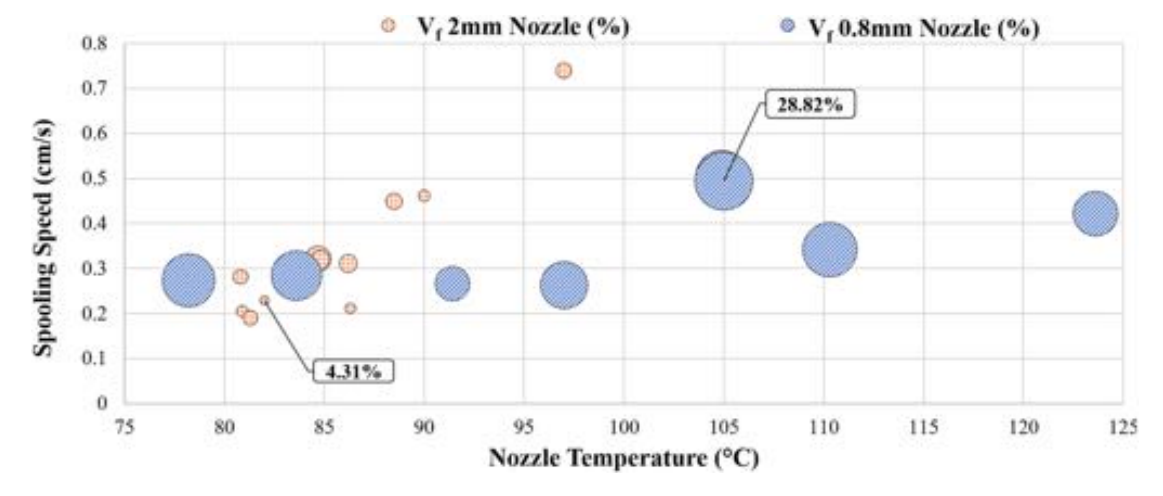


Fig. 4. Effects of spooling speed and nozzle temperature on the resulting filament V_f shown over the range of process parameters. The bubble radius reflects the V_f which ranged from 4.31 % to 28.82 %. The range of V_f values for the 0.8 and 2 mm nozzles are 24.35 \pm 3.40 and 7.1 \pm 2.15.

C. Marquis et al. Materials & Design 235 (2023) 112411

standard deviations in $V_{\rm f}$ for the 0.8 and 2 mm nozzles were 3.4 % and 2.15 %, respectively, and the resulting coefficients of variation in $V_{\rm f}$ for these two nozzles were 14 % and 30 %, respectively. Clearly, small changes in the amount of matrix coating the fibers produce large changes in the total $V_{\rm f}$.

The 0.8 mm nozzle resulted in the largest V_f of fibers as well as the largest degree of variation about the mean. Large V_f is preferred for maximizing strength, but it decreases the filament printability, especially if the concentration of fibers becomes too high. The V_f also contributes to the fiber distribution across the filament as shown in Fig. 5. Fig. 5a shows a hypothetical cross-section with random distribution of fibers, in comparison to filaments produced without (5b) and with (5c) fiber dispersion. By identifying the location of fibers with respect to the filament centroid it was possible to quantify the homogeneity in reinforcement as a function of distance from the centroid (Fig. 5d). The fiber probability distribution exhibits a shift to the right with dispersion, indicating a more random and homogenous distribution of the fibers within the matrix. The Gaussian fit parameters for filaments produced using these conditions are listed in Table 1.

The value of μ in Table 1 for the fit indicates the midpoint of the gaussian profile. The filament without dispersion has a midpoint of 0.415 (normalized distance) in comparison to 0.655 with dispersion. More fibers are located near the surface of the filament when processing was performed with fiber dispersion.

A comparison of representative filaments before and after printing is shown in Fig. 6. As evident from this image, although the fibers are dispersed in the filament before printing, they become agglomerated near the center after printing. This redistribution causes regions of high V_f near the center and regions without fibers at the periphery. The lower relative viscosity of the PCL matrix enables it to be displaced adjacent to the central fiber tow. Despite the nonuniform fiber dispersion the filament and printed samples exhibit low porosity, with no microscopic voids present. This is noteworthy as porosity is a common characteristic of 3D printing by FFF [37].

Fig. 7 presents stress strain responses for the UPE/PCL composite filament produced with fiber dispersion compared to the UHMWPE yarn as a control. Clearly there is some variation in the elastic response and the strength of the material in both conditions. The degree of variability

 Table 1

 Gaussian fit parameters for the fiber dispersion (Eq. (1)).

	Α	μ	σ
2 mm w/o DF	7.867	0.415	0.270
2 mm w/DF	7.526	0.655	0.298

in properties of the fiber tow and UPE/PCL filament are very similar. Most notable in Fig. 7, the strength of the composite filament is substantially lower than that of the yarn, which is expected due to the low $V_{\rm f}$.

The stress-strain responses for the filaments with and without fiber dispersion in the as-pultruded condition are shown in Fig. 8a and b, respectively. Results for these two filaments after printing are shown in Fig. 8c and d, respectively. It is important to highlight that the stress represented in Fig. 8 is the "apparent fiber strength" as estimated according to Eq. (2). This description of the strength facilitates a more robust comparison with the respect to the fiber tow response in Fig. 7.

The average apparent fiber strength (UTS_{fiber}) and modulus of toughness (MOT) were estimated using the tensile responses presented in Fig. 8 and are shown in Fig. 9 for the two different conditions of fiber dispersion. The error bars presented in Fig. 9 signify the standard deviation of the measurements. Results for the UTS and the MOT are shown in Fig. 9a and b, respectively.

Properties for the neat UHMWPE yarn control are included to convey the extent of changes caused by processing and printing. The neat UHMWPE fibers exhibited a UTS of roughly 2900 ± 100 MPa. The apparent fiber strength in the filaments with and without dispersion for the unprinted condition were 2400 ± 160 MPa, and 2390 ± 170 MPa, respectively. In the printed condition, the apparent fiber strength with and without fiber dispersion was 1920 ± 250 MPa and 2220 ± 180 MPa, respectively, which represents decreases of approximately 20 % and 7 %.

Printing of the filament entails conduction of heat from the heater block and a gradient in temperature from the periphery of the filament in contact with the heater block canal to the center. The material with dispersed fibers underwent a larger reduction in strength, which is expected due to the increase in fiber proximity to the heater block. The

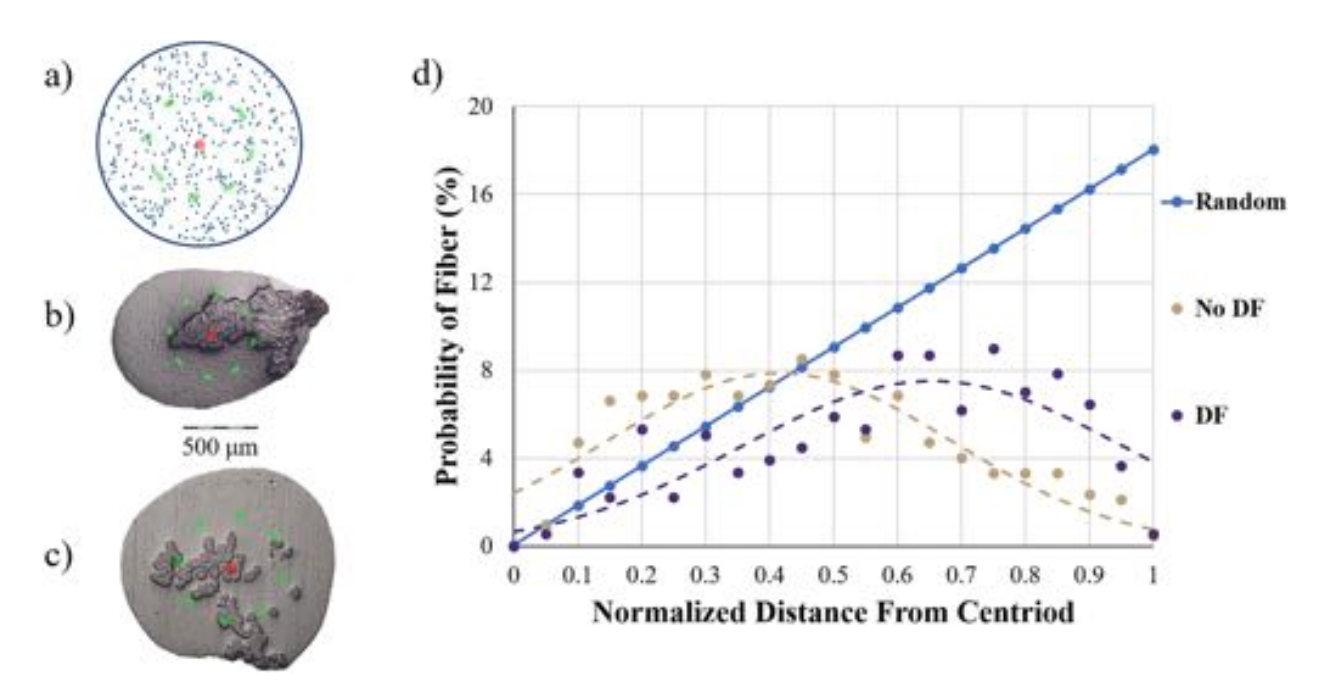


Fig. 5. Fiber dispersion within 2 mm filaments. a) Random distribution of fibers in filament, b) 2 mm filament without DF, c) 2 mm filament with DF; 10 % normalized diameter bin indicating the centroid (red), and 50 % normalized diameter bin (green). d) Probability of finding a fiber (%) vs Normalized distance from the centroid, dashed lines plot Gaussian fit. (For interpretation of the references to colour in this figure legend, the reader is referred to the web version of this article.)

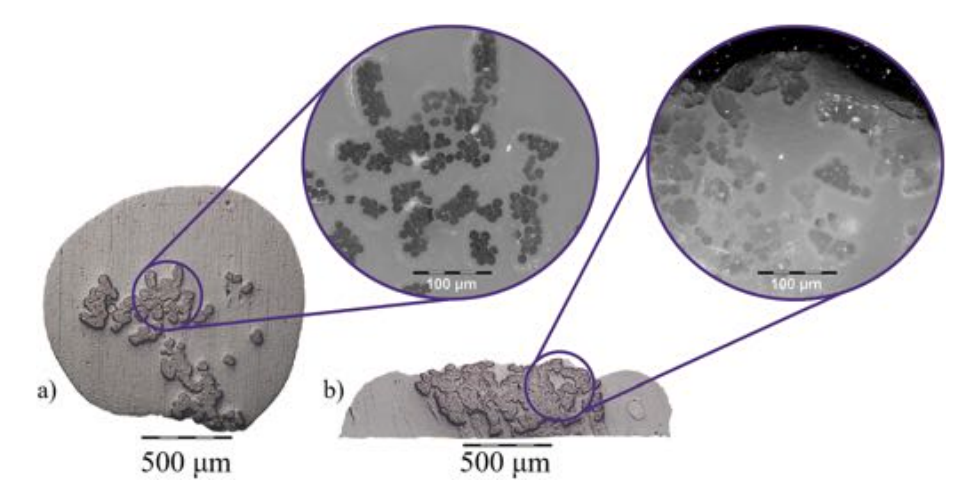


Fig. 6. Micrographs of the a) 2.0 mm filament ($V_f = 7$ %) with dispersed fibers before, and b) after printing through 1.2 mm nozzle ($V_f = 31.5$ %). Magnified regions of fibers are shown in darkfield.

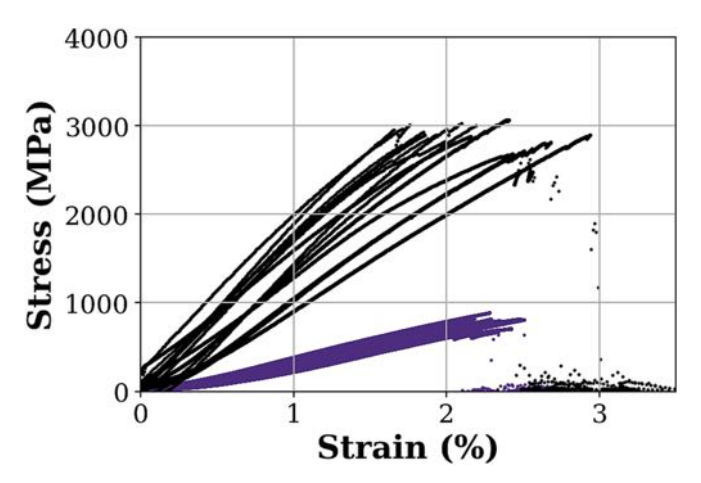


Fig. 7. Stress strain curves for neat UHMWPE yarn (black) and filament (purple) with dispersed fibers ($V_f=24\,$ %). Estimates of stress in this figure are based on the entire cross-section, including fibers and matrix. (For interpretation of the references to colour in this figure legend, the reader is referred to the web version of this article.)

high temperatures generated at the filament surface could introduce thermal degradation of the UHMWPE fibers, which is expected to cause the degradation in strength and/or strain to failure.

Regarding the changes in modulus of toughness, the neat UHMWPE displayed the highest MOT of $27\pm4~MJ/m^3$. The mean values for the unprinted filaments were $20\pm2~MJ/m^3$ and $24\pm3~MJ/m^3$ with and without dispersed fibers, respectively. In the printed condition, the system with dispersed fibers exhibited a MOT of $14\pm3~MJ/m^3$, a decrease of 35 %. Without fiber dispersion, the MOT decreased to $18\pm2~MJ/m^3$, a 25 % reduction. Hence, thermal degradation of the fibers incurred during printing appears to be more detrimental to the toughness than strength.

To understand contributions from processing defects to the variability in strength of the UPE/PCL, the two-parameter Weibull model was used to assess the distribution in UTS values for the apparent fiber strength before and after printing. Results are presented in Fig. 10.

Apart from the differences in strength imposed by processing with respect to the neat UHMWPE yarn, there are additional characteristics of note. The Weibull modulus (m), represented by the slope of the distribution, reflects the consistency in strength; higher slope = higher reliability. The highest Weibull modulus (m = 31.7) was achieved by the neat UHMWPE yarn, whereas the UPE/PCL filament samples with and

without dispersed fibers exhibited Weibull moduli of 16.6 and 16.3, respectively before printing. The printed filaments underwent a decrease in modulus to m=9.04 and m=14.5 with and without fiber dispersion, respectively. Clearly, the reliability was decreased by printing, which can be attributed to the thermal degradation of the fibers within the filaments, especially those near-surface in the dispersed condition.

4. Discussion

The UPE/PCL composite filament produced with fiber dispersion achieved an average UTS of 470±60 MPa in the printed condition. Without fiber dispersion, the UTS reached 550 \pm 45 MPa. These strengths are impressive for a compliant composite but are tempered by the relatively low V_f of fibers. Increasing the V_f within UPE/PCL filaments will be key to reach the high strength of the UHMWPE fibers. To obtain measures of performance that are more sensitive to the fiber condition the "apparent fiber strength" was evaluated. The printed filaments with fiber dispersion resulted in an average apparent fiber UTS of 1920±250 MPa. Without fiber dispersion, the apparent fiber UTS reached 2220 ± 180 MPa. These strengths are most representative of the load carrying capacity of the UHMWPE fibers and highlight the importance of increasing the V_f in future work. The UPE/PCL filament sets a new benchmark in strength for compliant fiber composites printed by FFF. The apparent fiber strength surpasses those reported in the open literature with tensile strengths that are generally substantially lower than 1000 MPa [24,38].

It is important to put the strength achieved by the UPE/PCE in perspective. There are commercial filaments for FFF with continuous fiber reinforcement. The most well-recognized include filaments with carbon fiber, glass fiber, and Kevlar fibers [39]. The ultimate tensile strength of these materials is quoted from the manufacturer as 800 MPa, 590 MPa, and 610 MPa, respectively [40]. Recent studies performed by Hu et al. [24] and Parker et al. [41] reported tensile strengths for the carbon fiber system of roughly 600 MPa. The lower strength in the printed condition is attributed to fiber damage [20,24,42]. A prototype composite filament produced by Toray that consists of high strength continuous carbon fibers with PPS matrix recently achieved a UTS of roughly 2 GPa after printing [20], which is a benchmark for continuous fiber composites printed by FFF. Having achieved an apparent fiber strength comparable to the strength of CCF/PPS, the UPE/PCL system has tremendous potential and appears limited only by the currently low V_f. However, there are some aspects of performance that warrant further discussion.

Printing of the UPE/PCL caused degradation in the mechanical

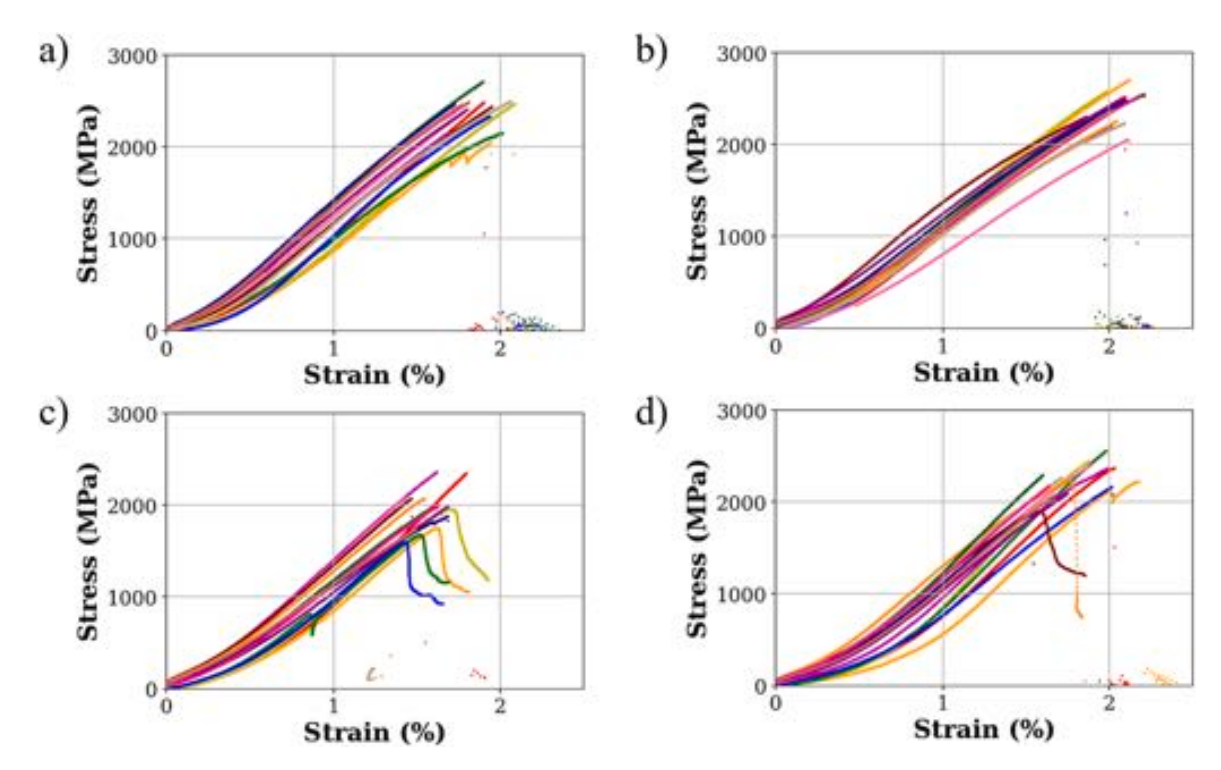


Fig. 8. Stress strain curves for the apparent fiber strength with $V_f = 24$ %. a) DF Filament, b) Filament W/O DF, c) DF Printed, d) Printed W/O DF. Note: Colors denote different test runs.

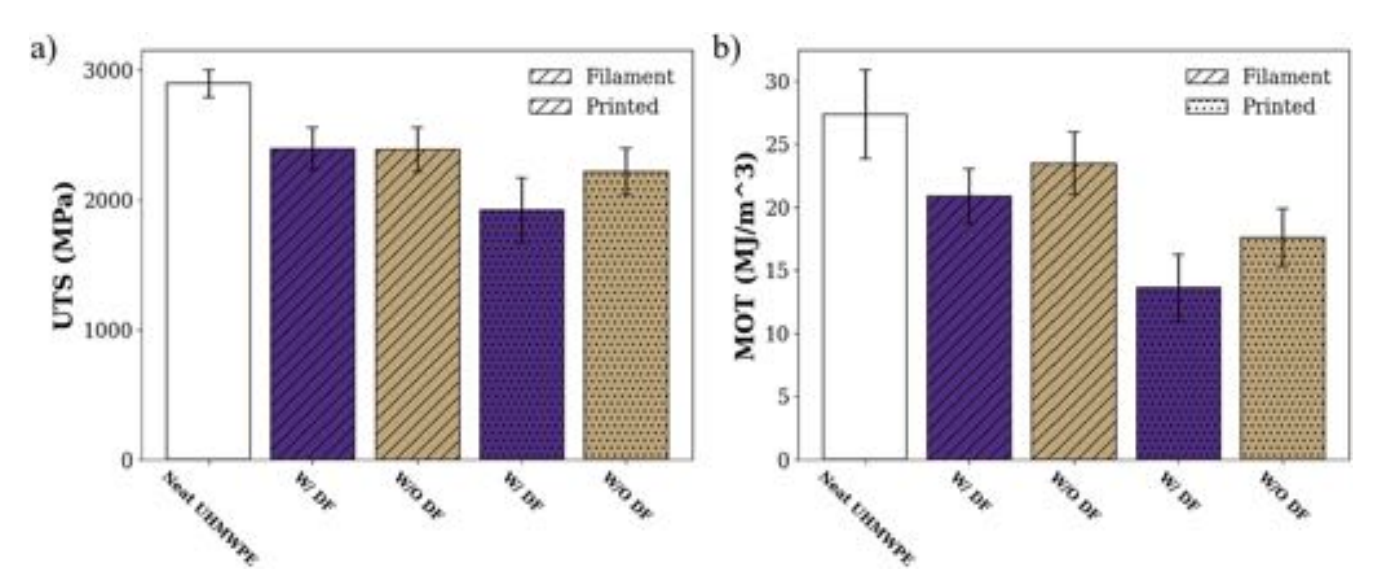


Fig. 9. Mechanical properties of the fibers before and after printing are shown in terms of the average with error bars representing the standard deviation where W/DF indicates with dispersed fibers and W/O DF indicates without dispersed fibers. a) Ultimate tensile strength (UTS), and b) Modulus of toughness (MOT).

properties with respect to that of the filament and with respect to the neat UHMWPE yarn. The reduction in apparent fiber strength of the filament with respect to the neat fibers ranged from 7 % (w/o DF) to 20 % (DF). The extent of damage is significantly less than that for carbon fiber filaments, which ranges from 10 to 60 % [20,24]. For the carbon fiber system, damage resulted from the concentrated rolling contact of the filament during extrusion, the sharp radius of curvature in the filament as it exits the nozzle and the ironing force transmitted from the nozzle to the deposited filament [20,24]. The compliant UHMWPE fibers and their greater extensibility facilitates printing with less mechanical degradation of the fiber tow overall. While the degradation in strength for carbon fiber filaments is postulated to be linked to damaged or

fractured fibers, the damage in the UPE/PCL is fundamentally different [20,24]. Degradation in the UPE/PCL is hypothesized to be caused by the high temperature exposure of near-surface fibers to the nozzle body during printing. Indeed, there is evidence of fiber consolidation in Fig. 6 (b) near the surface exterior where the nozzle heat may have caused fusion of fibers into localized bundles. This fusion can create areas of concentrated stress and weaken the fibers. There was no apparent uniformity to the grouping of fused fibers throughout the sample interior or between processing steps.

Regarding the Weibull distributions in Fig. 10, there is a decrease in the modulus from $m\approx 32$ for the Neat UHMWPE yarn, to $m\approx 16$ for the filament, and $m\approx 9$ after printing. Clearly the reliability decreases after

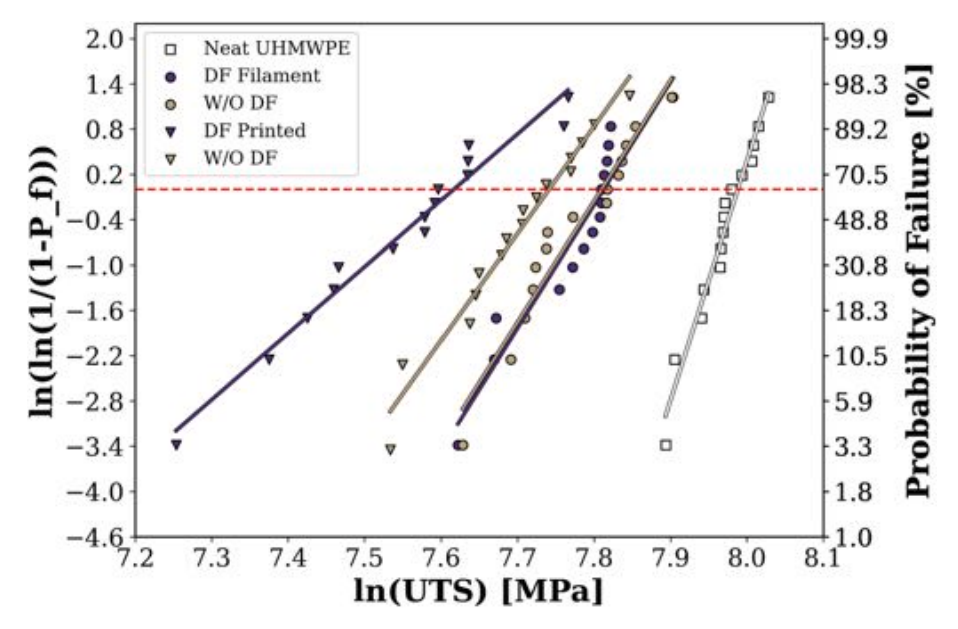


Fig. 10. Weibull plots for the apparent fiber strength in the filament prior to and after printing compared to the neat UHMWPE.

each step of processing of the UPE/PCL, which could hinder potential applications. While the UPE/PCL appears appropriate for applications requiring strength, toughness, and flexibility, it will be necessary to refine the fabrication of filaments and the printing process to improve reliability.

There are alternatives to developing composites with compliant fibers by pultrusion for FFF. Amza et al. [32] introduced UHMWPE fibers between consecutive printed layers of PLA, which resulted in UTS of 46-49 MPa, a 12-23 % increase over that for neat PLA [32]. But this method results in very low fiber volume fraction (1.16 %) when compared to the pultrusion approach, which yielded V_f herein of up to 24 %. The methods outlined by Zhang et al. use a 4-axis 3D printer that injects pultruded filaments directly through a custom nozzle assembly [43]. The methods of Matsuzaki et al. are also viable for developing continuous fiber composites by nozzle impregnation within the heated portion of the printer's extruder assembly [26]. He et al. adapts this approach for the fabrication of thermoset composites using direct ink writing practices to encapsulate fibers within resin by nozzle impregnation [44]. Zhang et al. enrolls a different approach for fabricating thermoset composites using electrostatic flocking and infrared melting to form filaments [45].

Apart from the recent work on printing with continuous carbon fibers, most composites printed by FFF achieve a UTS less than 10 % of the UPE/PCL [7,20,24,43]. Hence, results for the UPE/PCL highlight the promise of the pultrusion approach for producing continuous fiber reinforced thermoplastics with compliant UHMWPE fibers [43]. Of course, the fiber V_f is a key factor contributing to the axial strength of the printed composite materials, which is an admitted weakness of the current UPE/PCL system. A weak link in FFF of thermoplastic composites is the relatively low interfacial strength between the fiber and matrix [7]. A higher V_f of fibers will increase the dependency on the interfacial bonding surface area. Matsuzaki et al. proposed an upper limit on the V_f in FFF of roughly 50 %, which is slightly lower V_f than is characteristic of pre-impregnated materials [26]. The matrix content is key to layer fusion. Sizing of the fibers and cross linking between the fibers and matrix could be applied to improve the "interface-dependent" mechanical properties. The UPE/PCL filaments with 0.8 mm diameters possess a V_f of 24 %, roughly half the proposed maximum [26]. The current low V_f of the UPE/PCL can be overcome by introducing multiple fiber tows in filament production and this work is currently underway.

The microstructure of a two-layer uniaxial printed laminate

consisting of five adjacent contours is shown in Fig. 11.

There are two concerns with the microstructure in this figure, including large voids, and the agglomeration of fibers in discrete groups that are associated with the individual printed contours rather than an even dispersion. The voids are concerning due to the potential decrease in mechanical performance [19]. They appear to form from encapsulation of air pockets during printing. These voids can be reduced by printing at higher temperatures but increase the risk of thermal damage to the UHMWPE fibers. There are other defects evident in Fig. 11 including regions absent of PCL matrix around some fiber bundles and near the print surface where the matrix appears to have been scraped away. This feature results from tension in the fibers during printing and shear where the filament contacts the nozzle edge.

The UPE/PCL filaments can be printed with only limited difficulty and printed without segmentation of the fibers [46]. Fig. 12a shows a 5-ply cross-ply laminate consisting of $0^{\circ}/90^{\circ}$ stacking sequence. A detailed view of the microstructure is shown in Fig. 12b.

It is possible to produce complex geometries with this composite filament akin to those possible with other traditional FFF methods printing only neat resin. Nevertheless, the level of productivity in printing is currently limited. The laminates in Fig. 12 were printed using print speeds ranging from 10 to 50 mm/min. Prior to print head movement the matrix and fibers were secured by slightly lowering the nozzle closer to the print bed as outlined by Zhang et al., which enables the pultrusion to be automated [47]. Curved portions of the tool path required much slower printing speeds (10 mm/min) as the PCL matrix requires ample time to cool while the tool head moves around the arc. The solidified matrix acts as a pivot point for the compliant fibers to rotate about. While there was minimal deviation of the deposited filament from the tool path, the productivity was admittedly low. Future work must focus on increasing throughput if this approach will be industrially viable.

There are limitations to the present study that are important to consider. Clearly the fiber distribution in the printed filament is not uniform. Further development is required to increase the fiber dispersion throughout the PCL matrix. One method to improve uniformity is the addition of multiple fiber tows with a smaller tank nozzle. In theory, a smaller nozzle forces the matrix to percolate deeper into the fiber tows and removes additional excess matrix. The introduction of multiple fiber tows would also increase the overall fiber $V_{\rm f}$. In addition, the reduction in strength after printing highlights the need to reduce thermal damage

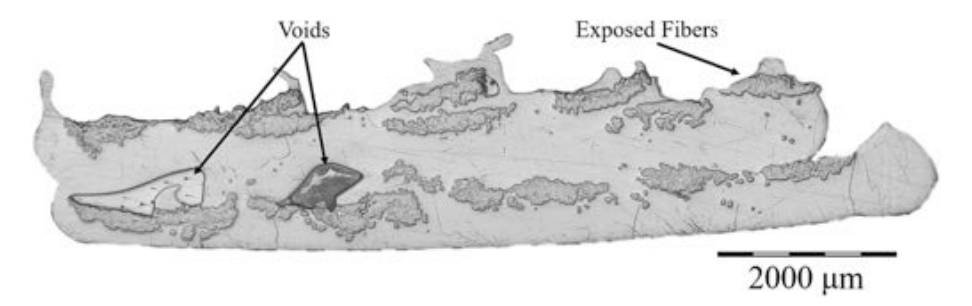


Fig. 11. Microstructure of two-layer print of UHMWPE reinforced PCL composite with five contours printed on each layer.

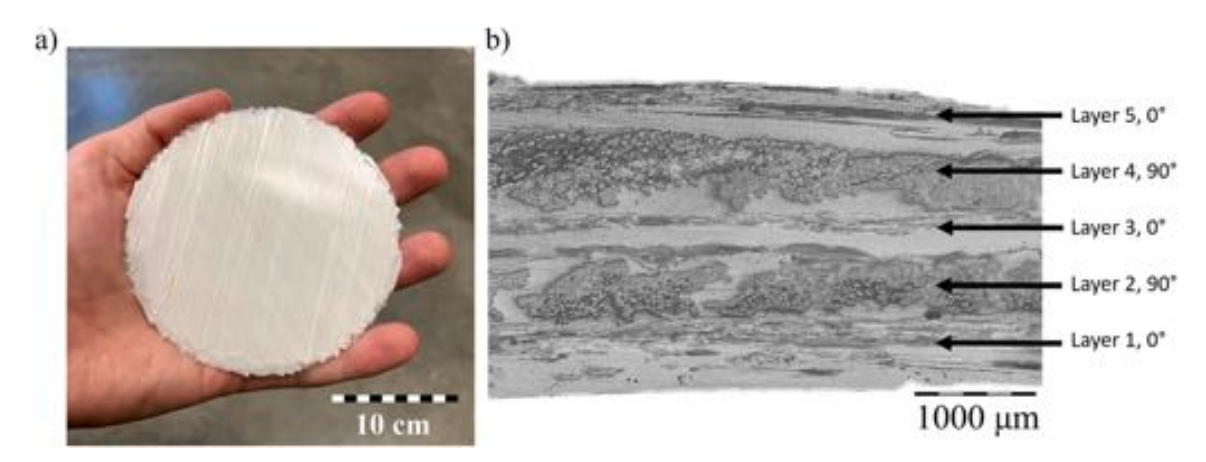


Fig. 12. Printing of laminates with the UPE/PCL filament. a) Net shape composite disk printed with 0/90° infill. b) Cross Section of a 5-layer disk printed with 0/90° stacking sequence.

of the fibers during filament fabrication and printing. Furthermore, this continuous fiber system poses challenges to the printing of parts with large z heights due to effects from the "ironing force". Contact of the nozzle with the printed substrate generates a moment at the top of the printed component that promotes delamination from the print bed, as noted by Zhang et al. [37]. These complications can be overcome.

The UPE/PCL composite, as well others in the family with UPE reinforcements, could substantially expand the design envelope for advanced structural applications. With further refinement and potential changes to the matrix material, this composite material could serve as a viable option for a variety of applications including medical grade prosthetics, tough-flexible multi-material joints, wearable electronics, and next generation flexible armors. The high strength and flexibility of the fiber reinforcement will support a multi-functionality in printed components that is presently not achievable with the traditional composite materials involving stiff fibers.

5. Conclusion

In conclusion, composite filaments of UHMWPE yarn within a PCL matrix were produced for fused filament fabrication (FFF). The material was successfully printed by FFF with two different configurations, i.e., with and without fiber dispersion. The virgin filament demonstrated an ultimate tensile strength (UTS) that exceeded 590 MPa prior to printing. After printing the minimum average UTS reached 474 MPa, which is the highest reported strength of a continuous fiber composite with compliant fibers printed by FFF. Printing resulted in degradation of the material, which was most extensive in the dispersed fiber condition, with up to 20 % reduction in UTS and nearly 40 % reduction in the MOT. Weibull distributions for the strength showed that printing also caused a reduction in reliability. The reduction in strength and reliability appears to be related to thermal degradation of the UHMWPE fibers, which was most extensive in the filament produced with dispersed fibers.

Improvements in resistance to thermal damage and increasing the printability are needed to expand the utility of this novel continuous composite filament.

Declaration of Competing Interest

The authors declare that they have no known competing financial interests or personal relationships that could have appeared to influence the work reported in this paper.

Data availability

Data will be made available on request.

Acknowledgements

The authors acknowledge that this study was made possible through partial support from the Joint Center for Aerospace Technology Innovation (JCATI), the ARCS Foundation and a College of Engineering Fellowship from the University of Washington (UW) to C. Marquis. The authors acknowledge Ellie Enebo for her contributions to the graphical abstract and Anushka Sarode of the UW for her contributions to the figures.

References

- Wohlers T., 2014. "Wohlers report 2014: 3D printing and additive manufacturing, state of the industry, annual worldwide progress report," Wohlers Associates Incorporated.
- [2] S. Senei, D. Popescu, 3D-printed of carbon fiber reinforced polymer composites: a systematic review, Composites Science 4 (2020) 98, https://doi.org/10.3390/ jcs4030098.
- [3] X. Yan, P. Gu, A review of rapid prototyping technologies and systems, Computer-Aided Design 28 (1996) 307–318.

- [4] B. Berman, 3-D printing: The new industrial revolution, Business Horizons 55 (2) (2012) 155–162.
- [5] P. Zhuo, S. Li, I. Ashcroft, A. Jones, Material extrusion additive manufacturing of continuous fibre reinforced polymer matrix composites: A review and outlook, Composites Part B: Engineering 224 (2021), 109143, https://doi.org/10.1016/j. compositesb.2021.109143.
- [6] X. Wang, M. Jiang, Z. Zhou, J. Gou, D. Hui, 3D printing of polymer matrix composites: A review and prospective, Composites Part B: Engineering 110 (2017) 442–458
- B. Brenken, E. Barocio, A. Favaloro, V. Kunc, R. Pipes, Fused filament fabrication of fiber-reinforced polymers: A review, Additive Manufacturing 21 (2018) 1–16, https://doi.org/10.1016/j.addma.2018.01.002.
- [8] J. Frketic, T. Dickens, S. Ramakrishnan, Automated manufacturing and processing of fiber-reinforced polymer (FRP) composites: An additive review of contemporary and modern techniques for advanced materials manufacturing, Additive Manufacturing 14 (2017) 69–86, https://doi.org/10.1016/j.addma.2017.01.003.
- [9] P. Zhang, S. Sun, J. Duan, H. Fu, Z. Han, H. Geng, Y. Feng, Line width prediction and mechanical properties of 3D printed continuous fiber reinforced polypropylene composites, Additive Manufacturing 61 (2023), 103372, https://doi.org/10.1016/ j.addma.2022.103372.
- [10] P. Parandoush, D. Lin, A review on additive manufacturing of polymer-fiber composites, Composite Structures 182 (2017) 26–53.
- [11] H. Tekinalp, et al., Highly oriented carbon fiber–polymer composites via additive manufacturing, Compos Sci Technol 105 (2014) 144–150.
- [12] W. Zhong, F. Li, Z. Zhang, L. Song, Z. Li, Short fiber reinforced composites for fused deposition modeling, Materials Science and Engineering A 301 (2001) 125–130.
- [13] A. Dickson, J. Barry, K. McDonnell, D. Dowling, Fabrication of continuous carbon, glass and Kevlar fibre reinforced polymer composites using additive manufacturing, Additive Manufacturing 16 (2017) 146–152, https://doi.org/ 10.1016/j.addma.2017.06.004.
- [14] J. Chacón, M. Caminero, P. Núñez, E. Plaza, I. Garcia-Moreno, J. Reverte, Additive manufacturing of continuous fibre reinforced thermoplastic composites using fused deposition modelling: effect of process parameters on mechanical properties, Composites Science and Technology 181 (2019), 107688, https://doi.org/ 10.1016/j.compscitech.2019.107688.
- [15] C. Hsueh, Young's modulus of unidirectional discontinous-fibre composites, Compos Sci Technol 60 (2000) 2671–2680.
- [16] C. Tucker, E. Liang, Stiffness predictions for unidirectional short-fiber composites: Review and evaluation, Compos Sci Technol 59 (5) (1999) 655–671.
- [17] P. Hine, H. Lusti, A. Gusev, Numerical simulation of the effects of volume fraction, aspect ratio and fibre length distribution on the elastic and thermoelastic properties of short fibre composites. Compos Sci Technol 62 (2002) 1445–1453.
- [18] F. Safari, A. Kami, V. Abedini, 3D printing of continuous fiber reinforced composites: a review of the processing, pre- and post-processing effects on mechanical properties, Polymers and Polymer Composites 30 (2022) 1–26, https://doi.org/10.1177/09673911221098734.
- [19] S. Wickramasinghe, T. Do, P. Tran, FDM-Based 3D printing of polymer and associated composite: A review on mechanical properties, defects and treatments, Polymers 12 (2020) 1529, https://doi.org/10.3390/polym12071529.
- [20] M. Parker, A. Inthavong, E. Law, S. Waddell, N. Ezeokeke, R. Matsuzaki, D. Arola, 3D printing of continuous carbon fiber reinforced polyphenylene sulfide: Exploring printability and importance of fiber volume fraction, Additive Manufacturing 54 (2022), 102763, https://doi.org/10.1016/j.addma.2022.102763.
- [21] N. Li, Y. Li, S. Liu, Rapid prototyping of continuous carbon fiber reinforced polylactic acid composites by 3D printing, Materials Processing Technology 238 (2016) 218–225, https://doi.org/10.1016/j.jmatprotec.2016.07.025.
- [22] X. Tian, T. Liu, C. Yang, Q. Wang, D. Li, Interface and performance of 3D printed continuous carbon fiber reinforced PLA composites, Composites: Part A 88 (2016) 198–205, https://doi.org/10.1016/j.compositesa.2016.05.032.
- [23] G. Melenka, B. Cheung, J. Schofield, M. Dawson, J. Carey, Evaluation and prediction of the tensile properties of continuous fiber-reinforced 3D printed structures, Composite Structures 153 (2016) 866–875, https://doi.org/10.1016/j. compstruct.2016.07.018.
- [24] Y. Hu, R. Ladani, M. Brandt, Y. Li, A. Mouritz, Carbon fiber damage during 3D printing of polymer matrix laminates using the FDM process, Materials & Design 205 (2021).
- [25] H. Zhang, D. Liu, T. Huang, Q. Hu, H. Lammer, Three-dimensional printing of continuous flax fiber-reinforced thermoplastic composites by five-axis machine, Materials. 13 (7) (2020) 1678, https://doi.org/10.3390/ma13071678.
- Materials. 13 (7) (2020) 1678, https://doi.org/10.3390/ma13071678.
 [26] R. Matsuzaki, M. Ueda, M. Namiki, T.K. Jeong, H. Asahara, K. Horiguchi, T. Nakamura, A. Todoroki, Y. Hirano, Three-dimensional printing of continuous-fiber composites by in-nozzle impregnation, Scientific Report 6(1) (2016).

- [27] T. Fruleux, M. Castro, P. Sauleau, R. Matsuzaki, A. Duigou, Matrix stiffness: A key parameter to control hydro-elasticity and morphing of 3D printed biocomposite, Composites Part A: Applied Science and Manufacturing 156 (2022), 106882, https://doi.org/10.1016/j.compositesa.2022.106882.
- [28] Y. Huang, X. Tian, Z. Zheng, D. Li, A. Malakhov, A. Polilov, Multiscale concurrent design and 3D printing of continuous fiber reinforced thermoplastic composites with optimized fiber trajectory and topological structure, Composite Structures 285 (2022), https://doi.org/10.1016/j.compstruct.2022.115241.
- [29] C. Liu, P. Hung, Effect of the infill density on the performance of a 3D-printed compliant finger, Materials & Design 223 (2022), https://doi.org/10.1016/j. matdes 2022 111203
- [30] DSM. (n.d.). Dyneema® fiber. @dyneema. Retrieved December 15, 2022, from https://www.dsm.com/dyneema/en_GB/our-products/dyneema-fiber.html.
- [31] T. Tam, A. Bhatnagar, Lightweight ballistic composites (Second Edition): High-performance ballistic fibers and tapes, Woodhead Publishing Series in Composites Science and Engineering (2016) 1–39.
- [32] Amza, C., Zapciu, A., Eypórsdóttir, A., Björnsdóttir, A., Borg, J., 2019. "Embedding ultra-high-molecular-weight polyethylene fibers in 3D-printed polylactic acid (PLA) parts," *Polymers* (Basel).
- [33] R. Matsuzaki, T. Nakamura, K. Sugiyama, M. Ueda, A. Todoroki, Y. Hirano, Y. Yamagata, Effects of set curvature and fiber bundle size on the printed radius of curvature by a continuous carbon fiber composite 3D printer, Additive Manufacturing 24 (2018) 93–102, https://doi.org/10.1016/j.addma.2018.09.019.
- [34] Universal testing systems, fixtures, and accessories. ADMET. (n.d.). Retrieved December 12, 2022, from https://www.admet.com/products/test-fixtures-and-accessories/test-fixtures/rope-and-thread/.
- [35] S. Eshraghi, S. Das, Mechanical and microstructural properties of polycaprolactone scaffolds with one-dimensional, two-dimensional, and three-dimensional orthogonally oriented porous architectures produced by selective laser sintering, Acta Biomaterialia 6 (7) (2010) 2467–2476, https://doi.org/10.1016/j. actbio.2010.02.002.
- [36] Beckman, I., Lozano, C., Freeman, E., Riveros, G., 2021. "Fiber selection for reinforced additive manufacturing," Polymers, Volume 13, no. 14.
- [37] M. Yamawaki, Y. Kouno, Fabrication and mechanical characterization of continuous carbon fiber-reinforced thermoplastic using a preform by threedimensional printing and via hot-press molding, Advanced Composite Materials 27 (2) (2018) 209–219, https://doi.org/10.1080/09243046.2017.1368840.
- [38] F. Kabir, K. Mathur, A.M. Seyam, A critical review on 3D printed continuous fiber-reinforced composites: History, mechanism, materials and properties, Composite Structures 232 (2020), 111476, https://doi.org/10.1016/j.compstruct.2019.111476.
- [39] M. Caminero, J. Chacón, I. García-Moreno, G. Rodríguez, Impact damage resistance of 3D printed continuous fibre reinforced thermoplastic composites using fused deposition modelling, Composites Part B: Engineering 148 (2018) 93–103. https://doi.org/10.1016/j.compositesb.2018.04.054.
- [40] Markforged. (n.d.). Material DATASHEET composites. Markforged Material Data Sheet. Retrieved December 15, 2022, from.
- [41] M. Parker, N. Ezeokeke, R. Matsuzaki, D. Arola, Strength and its variability in 3D printing of polymer composites with continuous fibers, Materials & Design 225 (2023), 111505, https://doi.org/10.1016/j.matdes.2022.111505.
- [42] J. Lozada, H. Garza, P. Castanon, W. Verbeeten, D. Saiz-Gonzalez, Tensile properties and failure behavior of chopped and continuous carbon fiber composites produced by additive manufacturing, Additive Manufacturing 26 (2019) 227–241, https://doi.org/10.1016/j.addma.2018.12.020.
- [43] K. Zhang, H. Zhang, J. Wu, J. Chen, D. Yang, Improved fibre placement in filament-based 3D printing of continuous carbon fibre reinforced thermoplastic composites, Composites Part A: Applied Science and Manufacturing 107454 (2023), https://doi.org/10.1016/j.compositesa.2023.107454.
- [44] X. He, Y. Ding, Z. Lei, S. Welch, W. Zhang, M. Dunn, K. Yu, 3D printing of continuous fiber-reinforced thermoset composites, Additive Manufacturing 40 (2021), 101921, https://doi.org/10.1016/j.addma.2021.101921.
- [45] H. Zhang, K. Zhang, A. Li, L. Wan, C. Robert, C. Bradaigh, D. Yang, 3D printing of continuous carbon fibre reinforced powder-based epoxy composites, Composite Communications 33 (2022), 101239, https://doi.org/10.1016/j. coco.2022.101239.
- [46] N. Suksangpanya, N. Yaraghi, D. Kisailus, P. Zavattieri, Twisting cracks in Bouligand structures, Journal of the Mechanical Behavior of Biomedical Materials 76 (2017) 38–57, https://doi.org/10.1016/j.jmbbm.2017.06.010.
- [47] Z. Zhang, Y. Long, Z. Yang, K. Fu, Y. Li, An investigation into printing pressure of 3D printed continuous carbon fiber reinforced composites, Composites Part A: Applied Science and Manufacturing 162 (2022), 107162, https://doi.org/10.1016/ i.compositesa.2022.107162.